Robert Kasper (Autor)

Numerical modeling and simulation of particulate fouling on structured heat transfer surfaces using multiphase Eulerian-Lagrangian LES

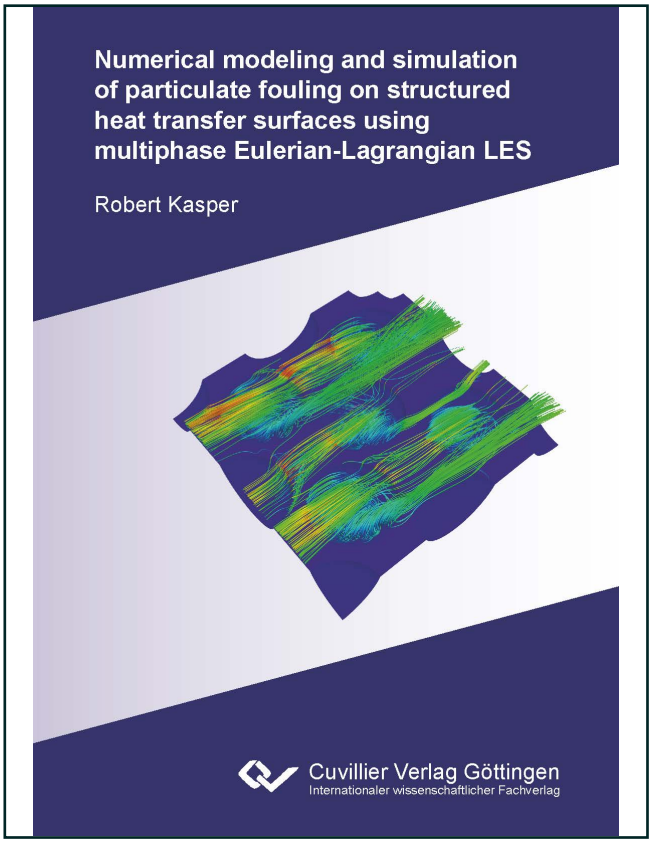

https://cuvillier.de/de/shop/publications/8442

1 Introduction

1.1 Motivation

The prediction and prevention of fouling is a crucial problem in many industrial processes, such as chemical and process industry, including oil refineries, power generation, energy recovering etc. Fouling, generally defined as the unwanted accumulation of various materials on solid surfaces of processing equipment, causes tremendous problems such as production loss, fuel and maintenance costs [139, 108]. Besides crystallization fouling, particulate fouling due to the deposition of small suspended particles (e.g., clay or iron oxide) and gravitational settling of larger particles is the most important and frequent fouling phenomena [17]. This is especially typical for heat exchangers, shown in Fig. 1.1, illustrating structured surfaces as rib turbulators, pin-fins arrays, protrusions or dimples extensively used to enhance the convective heat transfer [84]. The intensification of heat transfer is achieved by generating secondary flows which interfere the boundary layer growth as well as cause flow recirculation and shear-layer reattachment, promoting mixing and an increase of the turbulence intensity. On the other hand, besides the additional hydraulic losses due to the surface structuring, one of the major disadvantages of structured heat transfer surfaces is the susceptibility for particulate fouling, resulting in a significant reduction of the thermo-hydraulic performance over time.

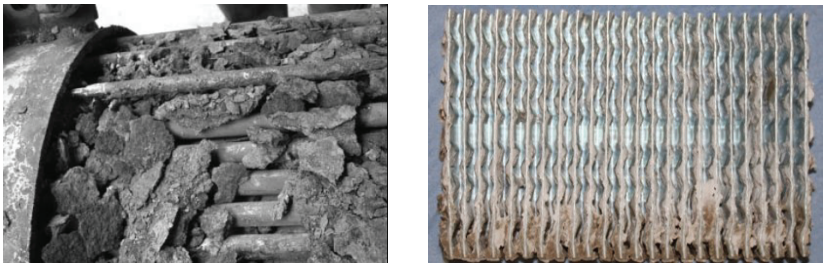

Fig. 1.1: Formation of fouling deposits inside a shell and tube heat exchanger (left) [109]; particulate fouling in a compact heat exchanger for automotive applications (right). Printed by permission from the ICTV, TU Braunschweig.

Various types of structured heat transfer surfaces have been thoroughly investigated with the objective to promote the heat transfer with a minimum hydraulic pressure loss.

Since the application of dimpled surfaces is a very efficient technique to enhance the thermo-hydraulic performance, as shown in Fig. 1.2, they are still primary subject of many experimental and numerical investigations in the field of thermo-fluid dynamics.

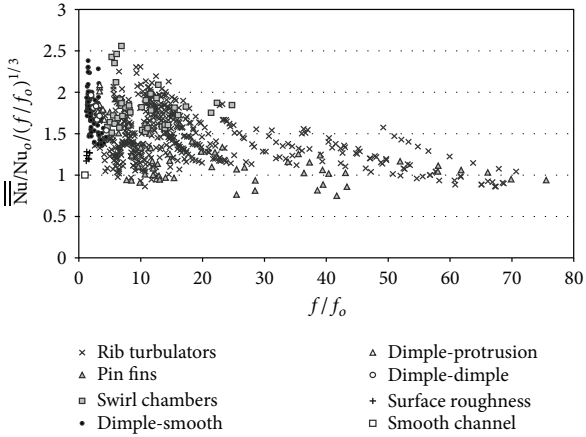

Fig. 1.2: Comparison of the globally averaged thermo-hydraulic performance dependent upon friction factor ratios for various heat transfer enhancement techniques [83].

Experimental studies were performed by Afanasyev et al. [2], who observed a maximum heat transfer augmentation of about 40% accompanied by a low increase of hydraulic losses for a plate with dimples in the turbulent regime, and by Chyu et al. [23], who evaluated the hydraulic losses and heat transfer enhancement for surfaces with an array of hemisphere and tear-drop shaped cavities in the range of Reynolds number, based on the hydraulic diameter of the channel, of $10{,}000 \leq Re_{D_h} \leq 50{,}000$. The results showed that both kinds of concavity configurations induce a heat transfer enhancement up to 2.5 in contrast to the opposite smooth wall whereas the flow resistance was half of that for rib tabulators. The effect of the channel height and dimple depth on heat transfer within the turbulent flow regime has been studied by Mahmood [95] and Ligrani et al. [85, 84]. Comprehensive numerical investigations regarding dimpled surfaces were published by Isaev et al. [62], who performed a study on the influence of the Reynolds number and dimple depth on the turbulent heat transfer and hydraulic loss in a narrow channel using URANS (unsteady Reynolds-averaged Navier-Stokes equations), by Elyyan et al. [42] as well as by Turnow et al. [148, 149]. Especially the numerical study of Turnow [146] and the experimental investigation of Kozlov and Chudnovsky [75] are very interesting, since they mention not merely the superior thermo-hydraulic performance of dimpled surfaces compared to other heat transfer enhancement techniques, but also a possible fouling-mitigation potential or self-cleaning process due to dimples. Kozlov and Chudnovsky explain the fouling mitigation with a tornado-like flow inside the dimple, as illustrated in Fig. 1.3,

which directly transports or evacuates approaching fouling particulates out of the dimple back into the core flow. However, it could be shown later by Turnow et al. [148, 146] that tornado-like spatial flow structures can be revealed by the spatial eigenmodes of the velocity field obtained from proper orthogonal decomposition (POD), but they do not exist as pure coherent flow structures. Further current experimental [155, 72, 9] and numerical results [88, 147, 87] show present significance of fundamental studies exploring advantages and disadvantages of dimpled surfaces.

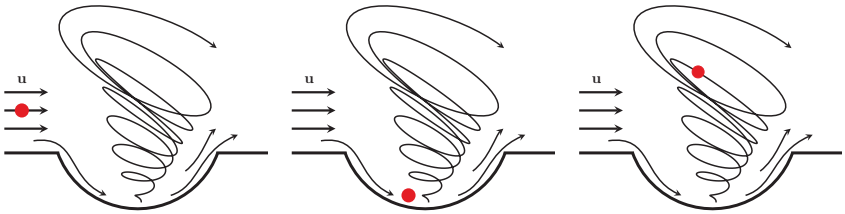

(a) Approach **(b)** Involve **(c)** Evacuation

Fig. 1.3: Mechanism of fouling mitigation through dimpled surfaces, according to Kozlov and Chudnovsky [75].

In contrast to this, investigations of structured heat transfer surfaces considering particulate fouling are relatively seldom. Available studies of particle-laden flows over non-flat surfaces, which emphasize the influence of surfaces curvature on the particle statistics as well as on particle accumulation and deposition, are presented by Marchioli et al. [97], Milici et al. [105] or De Marchis et al. [29], who investigated the influence of corrugated surfaces or roughnesses on particle dynamics in turbulent channel flows. A recent study is presented by Luo et al. [92], who analyzed effect of staggered arranged hemispherical roughness elements on a turbulent particle-laden flow. The most fundamental fouling modeling approach was proposed by Kern and Seaton [69], modeling the fouling processes as a balance between deposition and removal process. Further fouling models are described by Suitor et al. [141], Epstein [43], Bohnet [15] and Bott [17], but they allow only an integral fouling evaluation without accounting for local flow features and critical flow conditions (e.g., hot spots or low velocity zones). Latest numerical contributions are from Tong et al. [144], who simulated two-dimensional particle deposition and removal processes on tubes by coupling a multiple-relaxation-time lattice Boltzmann method with a finite volume procedure, and Wang et al. [159, 160] with a parameter study on the fouling characteristic of H-type finned heat exchanger using a two-dimensional RANS approach.

1.2 Fouling of heat transfer surfaces

The reasons and mechanisms of deposition formations on heat transferring surfaces are extremely manifold. Thus, the different types of fouling are usually subdivided into five main categories based on the underlying key physical/chemical processes [44, 15, 17, 108]:

Crystallization fouling Precipitation and deposition of dissolved salts, which at process conditions become supersaturated at the heat transfer surface or solidification fouling due to the shortfall of the solidification temperature of a dissolved component (e.g., solidification of wax from crude oil streams).

Particulate fouling Deposition of small suspended particles on heat transfer surfaces of any orientation and/or gravitational settling of larger particles onto horizontal surfaces.

Chemical reaction fouling Deposition formations at heat transfer surfaces by a chemical reaction, whereby the surface material itself is not part of the chemical reaction.

Corrosion fouling Formation of a corrosion layer on heat transfer surfaces which usually causes a low (additional) thermal resistance due the relatively high thermal conductivity of oxides. However, the enhanced surface roughness may promote other kinds of fouling.

Biological fouling Development and deposition of organic films consisting of microorganisms and their products such as bacteria and the attachment and growth of macroorganisms (e.g., mussels, algae) on heat transfer surfaces.

In practice or rather under real conditions several fouling mechanisms appear simultaneously, nearly always being mutually reinforcing. One exception is the combination of particulate and crystallization fouling, where particles of the crystallizing matter accelerate fouling, whereas particles from the other material may lead to reduced fouling due to a weakening of the deposit formation [108]. All mentioned fouling mechanisms occur in the following five consecutive steps [44, 15, 108]:

Initiation period The initially high overall heat transfer coefficient of a new or cleaned heat exchanger often remains unchanged for a certain time (i.e., no fouling occurs). The duration of this initiation period depends on various parameters, e.g., temperature and surface roughness.

Mass transport Transport of at least one (fouling) key component to the heat transfer surface through the fluid bulk, which is mostly achieved by diffusion. In case of particle transport to the surface, the consideration of inertia effects as well as thermophoretic and turbophoretic (only for turbulent carrier flows) forces is required.

Attachment and formation As soon as the transport to the heat transfer surface is completed, the foulant must stick to the heat transfer surface (for particulate fouling) or react to the deposit forming substance (e.g., $CaCO_3$).

Removal Depending on the strength of the deposit, erosion or removal due to the fluid flow (i.e., shear stresses acting on the surface of the fouling layer) occurs immediately after the first formation of deposits.

Aging The strength of the fouling layer can change in time. This aging process is referred to as *aging* and can either increase or decrease the strength of the deposits.

1.2.1 Fouling resistance and fouling curves

Fouling on heat transfer surfaces is generally considered in the design process of heat exchangers by using the so-called *thermal fouling resistance* $R_{f,th}$ in the evaluation of the overall heat transfer coefficient U [109]. For a clean heat transfer surface, the heat flow resistance is defined as:

$$\frac{1}{U_0} = \frac{1}{h_1} + \frac{x_w}{k_w} + \frac{1}{h_2} = \frac{1}{h_1} + R_w + \frac{1}{h_2}, \tag{1.1}$$

in which h_1 and h_2 are the corresponding heat transfer coefficients of both heat exchanging fluids, x_w and k_w is the thickness and the thermal conductivity of the heat transfer surface (or wall), respectively, and R_w is the thermal resistance of the separating wall. Assuming that fouling occurs only on one side of the heat transfer wall, which is valid for many industrial applications, the overall heat flow resistance of the fouled surfaces is [110]:

$$\frac{1}{U_f} = \frac{1}{h_1} + \frac{x_w}{k_w} + \frac{1}{h_2} + \frac{x_f}{k_f} = \frac{1}{h_1} + R_w + \frac{1}{h_2} + R_{f,th}, \tag{1.2}$$

where x_f is the thickness of the fouling layer, k_f is the thermal conductivity of the foulant material and $R_{f,th}$ is the fouling resistance, which can be interpreted as additional thermal resistance due to fouling. For constant flow rates, the fouling resistance at any time is the difference between the actual heat transfer resistance and the initial (clean) heat transfer resistance:

$$R_{f,th} = \frac{1}{U_f(t)} - \frac{1}{U_0}. \tag{1.3}$$

The time-dependent overall heat transfer coefficient is calculated from

$$U(t) = \frac{Q(t)}{A \cdot \Delta T_{lm}(t)}, \tag{1.4}$$

with the logarithmic mean temperature difference ΔT_{lm} (see e.g., Incropera et al. [61]) and the heat flow rate Q, which is given by:

$$Q = \dot{m} \cdot c_p \cdot \Delta T, \tag{1.5}$$

where ΔT is the temperature difference of either the heating or cooling fluid, $\dot{m}$ is the mass flow rate and c_p is the corresponding heat transfer capacity. The thermal fouling resistance can be easily monitored without any interruption of the process but allows only an assessment of the integral fouling behavior, since the temperatures are only measured at the inlet and outlet for the heat exchanging fluids. However, investigations of operating industrial heat exchanger have shown that fouling often follows a decreasing or even asymptotic trend. Based on this observation, Kern and Seaton suggested modeling the fouling process as a balance between competing transport processes to and from the heat transfer surface, namely, deposition and removal [109]. Therefore, the accumulation of the

deposited fouling mass m_f per unit area[1] in time t is expressed as [69]:

$$\frac{\mathrm{d}m_f}{\mathrm{d}t} = \dot{m}_d - \dot{m}_r = \frac{\mathrm{d}R_{f,th}}{\mathrm{d}t}\rho_f k_f, \tag{1.6}$$

assuming that the thermal conductivity k_f and the density ρ_f of the fouling material remain constant with time and deposit thickness. Based on the Kern and Seaton model, Eq. (1.6), the *fouling curves* for three essentially different cases are shown in Fig. (1.4).

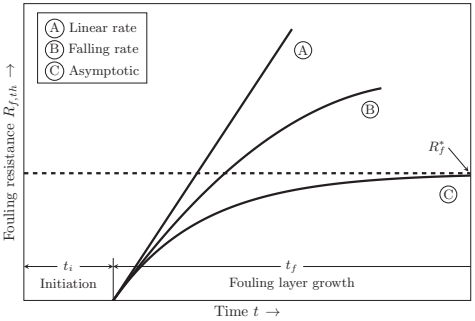

Fig. 1.4: Possible dependence of the fouling resistance $R_{f,th}$ on time t: idealized thermal fouling curves for a linear, falling and asymptotic growth rate.

Curve A shows a linear increase of the fouling resistance with time. This behavior is mainly observed when no removal of solids (i.e., $\dot{m}_r = 0\,\mathrm{kg/m^2s}$) takes place. For curve B, a slowing down (or falling rate) of the solids increase with increasing fouling layer thickness is observed, but without reaching a maximum. Curve C shows the characteristic asymptotic fouling behavior, which is , after a certain time, the solid removed per unit time and surface area is equal to the deposited solid (i.e., $\dot{m}_d - \dot{m}_r = 0\,\mathrm{kg/m^2s}$). Moreover, the mass of the fouling layer per unit area and thus also the fouling resistance reach limiting values, the so-called *asymptotic fouling resistance* $R^*_{f,th}$. Thereby, it is possible that, during the initial phase of fouling, the fouling resistance shows a linear increase [15].

1.2.2 Modeling of particulate fouling

Existing physically based models for the prediction of particulate fouling (see e.g., Müller-Steinhagen [109] or Bohnet [15]) are usually derived under the assumption that the growth of the fouling layer is leveled after a certain time. Following the pioneering work of Kern and Seaton [69], the progression of the fouling resistance with time can be expressed as:

$$\frac{\mathrm{d}R_{f,th}}{\mathrm{d}t}\rho_f k_f = \dot{m}_d - \dot{m}_r. \tag{1.7}$$

[1]Please note that the fouling mass m_f, the deposition rate $\dot{m}_d$ as well as the removal rate $\dot{m}_r$ are expressed as mass or mass flow rate per unit area (i.e., in $\mathrm{kg/m^2}$ and $\mathrm{kg/m^2s}$).

According to Müller-Steinhagen [109], the deposition rate $\dot{m}_d$ can be modeled through a simplified mass transfer correlation as being proportional to the bulk flow velocity u and the foulant concentration c:

$$\dot{m}_d = K_1 uc, \tag{1.8}$$

where K_1 is a (proportionality) model constant. Since the removal of deposited fouling material is mainly caused by shear forces from the bulk flow, the removal rate $\dot{m}_r$ is derived under the assumption that it is proportional to the shear stress τ_f acting on the surface of the fouling layer and to the thickness x_f of the fouling layer:

$$\dot{m}_r = K_2 \tau_f x_f, \tag{1.9}$$

with model constant K_2. Both modeling approaches are based on simplistic assumptions and ignore several mechanism that may be responsible for accumulation of fouling deposits on heat transfer surfaces and have therefore been frequently criticized, extended and improved. However, combining Eqs. (1.8) and (1.9) and integration with respect to time yields:

$$R_{f,th}(t) = \frac{K_1 uc}{\rho_f k_f K_2 \tau_f}\left(1 - e^{-K_2 \tau_f t}\right) = R^*_{f,th}\left(1 - e^{-bt}\right), \tag{1.10}$$

which includes the asymptotic fouling resistance $R^*_{f,th}$. This fundamental relationship describes the increase of the fouling resistance in time, which approaches the limiting value asymptotically. It is obvious that the final value of the fouling resistance increases with the foulant concentration in the carrier flow and decreases with the flow velocity, since the shear stress acting on the surface of the fouling layer is proportional to the square of the bulk flow velocity (i.e., $\tau_f \propto \rho u^2$). Moreover, Eq. (1.10) states that until the asymptotic fouling resistance is attained, the increase of the fouling resistance depends only on the bulk flow velocity as shown in Fig. 1.5.

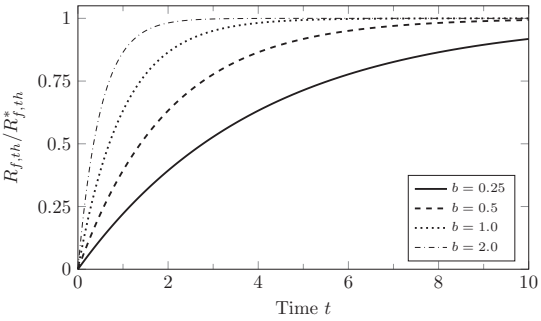

Fig. 1.5: Fouling resistance $R_{f,th}/R^*_{f,th}$ as a function of time t and parameter b in Eq. (1.10), according to the Kern and Seaton model [69].

Although the presented modeling approach, Eq. (1.10), provides essential information regarding the fouling process and reveals fundamental physical dependencies, it suffers from the drawback that it allows only a pure integral evaluation and assessment of particulate fouling without accounting for local flow features, e.g., switching vortices caused by dimples. Furthermore, a precise calibration of the model constants, which is based on experimental fouling investigations, is necessary to achieve reliable results.

1.3 Objectives and thesis outline

A careful review of the available literature has shown, that no numerical investigations of dimpled heat transfer surfaces regarding the interaction between local flow structures, convective heat transfer and fouling deposits using transient large-scale resolving numerical methods (e.g., LES or IDDES) exist at this moment. Moreover, the supposed fouling-mitigation potential of dimpled surfaces is still not confirmed numerically. This work is aimed to fill up this lack of knowledge by introducing a new multiphase Eulerian-Lagrangian approach which is suitable for CFD studies of heat transfer enhancement methods under consideration of particulate fouling using large-scale resolving methods, providing the opportunity to analyze the interaction between local flow structures and different fouling processes in a more comprehensive way. Thus, the two main objectives of this thesis are:

1. Development of a novel numerical approach for spatial- and time-resolved simulations of particulate fouling on structured heat transfer surfaces, based on Eulerian-Lagrangian LES. Extensive validation of the presented multiphase Eulerian-Lagrangian approach for canonical test cases (e.g., particle-laden backward-facing step flow, particle-laden channel flow).

2. Investigation of dimpled heat transfer surfaces regarding their ability to mitigate particulate fouling, while varying the dimple geometry (depth-to-dimple diameter ratio) and dimple arrangement (single spherical dimple and spherical dimples in a staggered arrangement, i.e., dimple package) as well as the carrier flow conditions (bulk flow velocity and mass loading of the dispersed phase).

This dissertation is divided into two parts. The first part contains the theoretical background including the derivation of the governing equations for the continuous phase (carrier flow) and the dispersed phase (foulant material), the numerical methodology as well as a description of the implemented fouling model. The second part presents the validation of the numerical methods and the results of the performed numerical fouling investigations for dimpled heat transfer surfaces followed by a conclusion.

2 Description of the continuous phase

In this chapter, the fundamental equations of fluid motions and heat transfer are derived, allowing a full description of the investigated incompressible carrier flows (i.e., continuous phase). Additionally, a condensed introduction into turbulent wall-bounded flows and different mathematical turbulence modeling approaches, with emphasis on the large-eddy simulation (LES), is given. More information and detailed discussions on fluid dynamics, turbulence, and modeling approaches for turbulent flows can be found in [89, 116, 123, 82, 124, 10].

2.1 Governing equations of fluid motion

The governing equations of fluid dynamics are derived under continuum assumption, which means that the considered fluid is a continuum state of matter and all flow variables can be defined at any point. This assumption holds for very small Knudsen numbers

$$Kn = \frac{\lambda}{L} \ll 1, \tag{2.1}$$

or more precisely, if the characteristic length scale of the flow L is much larger than the mean free path of the flow particles λ. In this case, the fluid motion is described through the principle of conservation of mass, momentum and energy expressed in a continuous way in space $\mathbf{x}$ and time t.

2.1.1 Continuity equation

Mass conservation implies that the mass of a fluid flow remains constant. Hence, for a fixed fluid-containing control volume $\mathrm{d}V$, the difference of the mass flow, which enters and leaves the considered control volume through its boundaries, is zero. This relation can be formulated using the following integral equation:

$$\frac{\partial}{\partial t}\int_V \rho \,\mathrm{d}V + \int_S \rho \mathbf{u}\cdot\mathbf{n}\,\mathrm{d}S = 0, \tag{2.2}$$

where ρ is the fluid density, $\mathbf{u}$ is the fluid velocity, $\mathrm{d}S$ is the infinitesimally small surface area and $\mathbf{n}$ is the unit vector orthogonal to $\mathrm{d}S$. The integral mass conservation, Eq. (2.2), can be transformed into the differential vector form by applying Gauss' divergence theorem,

see Eq. (4.6), to the convection term and introducing the del operator $\boldsymbol{\nabla}$:

$$\frac{\partial \rho}{\partial t} + \boldsymbol{\nabla} \cdot (\rho \mathbf{u}) = 0. \tag{2.3}$$

For incompressible or density-constant flows (i.e., flows in which ρ is independent both of space and time), as considered in this work, this equation reduces to:

$$\boldsymbol{\nabla} \cdot \mathbf{u} = 0. \tag{2.4}$$

Thus, the mass conservation is satisfied for incompressible flows with solenoidal (source- and sink-free) or divergence-free velocity fields.

2.1.2 Momentum equation

The momentum balance equation is based on Newtons second law of motion, stating that the temporal change of momentum inside a fixed fluid-containing volume of space $\mathrm{d}V$ is equal to the sum of all surface forces (e.g., pressure, normal and shear stresses) and body forces (e.g., gravity, centrifugal and Coriolis force) acting on the fluid in the considered control volume [46]. Thus, the integral form of the momentum equation becomes:

$$\frac{\partial}{\partial t} \int_V \rho \mathbf{u} \, \mathrm{d}V + \int_S \rho \mathbf{u}\mathbf{u} \cdot \mathbf{n} \, \mathrm{d}S = \int_S \mathbf{T} \cdot \mathbf{n} \, \mathrm{d}S + \int_V \rho \mathbf{B} \, \mathrm{d}V \,, \tag{2.5}$$

with the stress tensor $\mathbf{T}$, which is the molecular rate of transport of momentum, and vector $\mathbf{B}$, including the body forces (per unit mass). The surface integrals (convective and diffusive fluxes) need to be converted into volume integrals by applying Gauss' divergence theorem, which leads to following differential vector form of the momentum balance equation (Euler's first law of motion):

$$\frac{\partial \rho \mathbf{u}}{\partial t} + \boldsymbol{\nabla} \cdot (\rho \mathbf{u}\mathbf{u}) = \boldsymbol{\nabla} \cdot \mathbf{T} + \rho \mathbf{B}. \tag{2.6}$$

For Newtonian fluids the general stress tensor $\mathbf{T}$ is expressed by the static pressure and shear stresses, which results in:

$$\mathbf{T} = -\Big(p + \frac{2}{3}\mu \boldsymbol{\nabla} \cdot \mathbf{u}\Big)\mathbf{I} + 2\mu \mathbf{S}, \tag{2.7}$$

where μ is the dynamic viscosity, $\mathbf{I}$ is the identity tensor, p is the static pressure and $\mathbf{S}$ is the strain rate tensor:

$$\mathbf{S} = \frac{1}{2}\big(\boldsymbol{\nabla}\mathbf{u} + \boldsymbol{\nabla}\mathbf{u}^{\mathsf{T}}\big). \tag{2.8}$$